Journal of Power Sources 267 (2014) 104–116

Contents lists available at ScienceDirect

Journal of Power Sources

journal homepage: www.elsevier.com/locate/jpowsour

Purge gas recovery of ammonia synthesis plant by integrated configuration of catalytic hydrogen-permselective membrane reactor and solid oxide fuel cell as a novel technology

Fakhteh Siavashi [a, b], Majid Saidi [a], Mohammad Reza Rahimpour [a, *]

[a] Department of Chemical Engineering, School of Chemical and Petroleum Engineering, Shiraz University, Shiraz 71345, Iran
[b] National Iranian Oil Products Distribution Company (N.I.O.P.D.C), HSE Department, Tehran, Iran

HIGHLIGHTS

- A new configuration is proposed for purge gas recovery of ammonia synthesis plant.
- A membrane reactor is used to generate pure hydrogen as feed of SOFC.
- An electrochemical model for SOFC is developed.
- Parametric analysis of the membrane reactor and SOFC performance is done.

ARTICLE INFO

Article history:
Received 8 January 2014
Received in revised form
5 May 2014
Accepted 10 May 2014
Available online 22 May 2014

Keywords:
Purge gas
Catalytic reactor
Pd–Ag membrane
Solid oxide fuel cell
Methane steam reforming

ABSTRACT

The purge gas emission of ammonia synthesis plant which contains hazardous components is one of the major sources of environmental pollution. Using integrated configuration of catalytic hydrogen-permselective membrane reactor and solid oxide fuel cell (SOFC) system is a new approach which has a great impact to reduce the pollutant emission. By application of this method, not only emission of ammonia and methane in the atmosphere is prevented, hydrogen is produced through the methane steam reforming and ammonia decomposition reactions that take place simultaneously in a catalytic membrane reactor. The pure generated hydrogen by recovery of the purge gas in the Pd–Ag membrane reactor is used as a feed of SOFC. Since water is the only byproduct of the electrochemical reaction in the SOFC, it is recycled to the reactor for providing the required water of the reforming reaction. Performance investigation of the reactor represents that the rate of hydrogen permeation increases with enhancing the reactor temperature and pressure. Also modeling results indicate that the SOFC performance improves with increasing the temperature and fuel utilization ratio. The generated power by recovery of the purging gas stream of ammonia synthesis plant in the Razi petrochemical complex is about 8 MW.

1. Introduction

Nowadays environmental and energy challenges facing humanity are becoming two important factors that limited social and economic development. To satisfy the ever-increasing global energy demand, application of new environmentally friendly and highly economical approaches is necessary [1]. Hydrogen-based energy systems appear as an attractive alternative to common fossil fuel-based energy systems in the future. Hydrogen is an environmentally friendly replacement for other fuels in both industrial application and transportation [2]. Although hydrogen storage is difficult because of its low density, it has the largest energy of combustion per unit of mass. Its combustion with oxygen produces water and heat. So energy conversion devices using hydrogen are highly efficient and produce very little or no harmful emissions.

Fuel cells are electrochemical devices which convert the chemical energy of hydrogen to electricity power directly and produce pure water as the only byproducts. Among the various types of fuel cells, solid oxide fuel cell (SOFC) is more efficient [3]. SOFC is a kind of fuel cell contains two porous electrodes, which are separated by a nonporous oxide ion-conducting ceramic electrolyte. SOFC operates at temperatures about 800–1000 °C and uses hydrogen containing gas mixtures as a feed and oxygen in the air as

* Corresponding author. Tel.: +98 711 2303071; fax: +98 711 6287294.
E-mail address: rahimpor@shirazu.ac.ir (M.R. Rahimpour).

http://dx.doi.org/10.1016/j.jpowsour.2014.05.072
0378-7753/

an oxidant [4]. Although the high operating temperature of SOFC leads the flexibility of using various fuel types (i.e. methane, methanol, ethanol, biogas, etc.), SOFCs operate best on pure hydrogen. Since the concentration of pure hydrogen in the atmosphere is less than 1 ppm, hydrogen should be produced from other hydrogen containing fuels. Gasification of coal, reforming of hydrocarbons and electrolysis of water are several approaches for hydrogen production [5–12].

Since ammonia has high hydrogen content, it is introduced as an important source to generate hydrogen. Ammonia has many industrial applications, is commercially manufactured with Haber–Bosch process at temperature 450 °C and pressure about 250 atm [13]. Since the conversion per pass is not 100%, the reactor operates in loop mode. Ammonia is continuously condensed out of the loop and fresh synthesis gas is added. The synthesis gas contains small quantities of impurities such as methane and argon and also some impurities build up in the loop, so they must be continuously purged to atmosphere to prevent them from exceeding a certain concentration [14]. This purge gas stream which contains valuable hydrogen can be proposed as an appropriate feed for SOFC, but due to the presence of ammonia in this stream, direct application of this feed degrades the performance of anode electrode. Different studies considered pure ammonia as the feed of SOFC directly [15–18]. When oxygen ion conducting electrolyte is used in the SOFC, the presence of ammonia in the feed of SOFC increases the risk of producing NO_x compounds over anode catalyst as Eq. (1) [19]. Hence for preventing NO_x compounds, proton conducting electrolyte should be used when ammonia is fed to the fuel cell. Ammonia is decomposed as Eq. (2) at the cell temperature over anode that is consisting Ni-based material. As is shown in Eq. (2), ammonia is converted to hydrogen and nitrogen. The generated hydrogen undergoes electrochemical reaction at the anode-electrolyte interface and is converted to hydrogen ions and electrons. The protons pass the electrolyte and react to oxygen molecules and water is generated at the cathode-electrolyte interface [20].

$$2NH_3 + 5O^{2-} \rightarrow 2NO + 3H_2O + 10e^- \quad (1)$$

$$NH_3 \leftrightarrow \frac{3}{2}H_2 + \frac{1}{2}N_2 \quad (2)$$

Many researchers studied ammonia decomposition rate [21,22]. They found that dilute ammonia kinetic decomposition is slightly different from pure ammonia. For pure ammonia feed, the decomposition rate was found first order respect to ammonia partial pressure. But the inhibition effect of the hydrogen partial pressure is significant at low ammonia concentration (about ppm level) [23]. As reported in Table 1, the composition of ammonia in the purge gas of ammonia synthesis plant is not significant. So, not only the ammonia existing in the purge gas of ammonia synthesis plant is not decomposed over the anode, but also it is possible the reaction reverses and ammonia is produced in the cell. Hence the ammonia should be removed from the gas stream before entering to the cell.

Table 1
Characteristics of ammonia plant in the Razi petrochemical complex [37].

Ammonia plant specifications	Value
Number of ammonia units	2
Plant capacity	1000 (ton day^{-1})
Purge gas flow rate	285 (kg mol h^{-1})
Total ammonia in purge gas	1600 (ton $year^{-1}$)
Purge gas stream pressure	108.9 (bar)
Gas composition (mol %)	
NH_3	2.3
H_2	58.2
N_2	19.3
Ar	6.0
CH_4	14.2

Ammonia absorption by using water is a common approach to remove ammonia from the purge gas. In this way ammonia is scrubbed with water in an absorption tower at pressure about 75.5 bars. At this condition ammonia cannot remove perfectly and about 400 ppm ammonia remains in the purge gas stream [24]. Another approach is decomposition of ammonia in a catalytic reactor as Eq. (2). But the main challenge of this method is that due to high concentration of hydrogen and nitrogen in the purge gas stream, the decomposition reaction is limited thermodynamically, therefore ammonia conversion does not occur completely. The equilibrium limitation issue can be solved by using hydrogen-selective membrane which removes hydrogen from the reaction zone and shift the equilibrium of reaction toward right and as a result the conversion will increase. Rahimpour and Asgari studied the decomposition of ammonia over Ni/Al_2O_3 catalyst in a hydrogen-permselective membrane reactor to increase the conversion of ammonia in the purge gas stream and hydrogen production [25,26]. Their proposed model can be used for the design of an industrial catalytic membrane reactor for the removal of ammonia from the purge gas and production of hydrogen as a fuel of SOFC.

In addition to ammonia, there is an amount of methane in the purge gas. Methane is a greenhouse gas and has the most effect on the global warming [27]. It is usually burned in the flares to decrease its effect. Its reaction with steam is one of the most important processes to produce hydrogen. The methane steam reforming reaction is strongly endothermic and is conducted over Ni catalysts at high temperature conventionally. The reactions which occur during the methane steam reforming are as follows:

$$CH_4 + H_2O \leftrightarrow CO + 3H_2 \quad (3)$$

$$CO + H_2O \leftrightarrow CO_2 + H_2 \quad (4)$$

$$CH_4 + 2H_2O \leftrightarrow CO_2 + 4H_2 \quad (5)$$

According to Eqs. (3)–(5), an amount of carbon dioxide and carbon monoxide are produced as well as hydrogen. So the application of hydrogen-selective membrane reactor can produce pure hydrogen with high conversion of methane. Since the thermodynamic conditions of methane steam reforming reaction and decomposition of ammonia are similar, Eqs. (2)–(5) can be occurred simultaneously by adding required steam to purge gas in the catalytic membrane reactor.

Many researchers have investigated the methane steam reforming in a membrane reactor [6–9]. Due to good surface properties, high permeability and selectivity, high resistance to temperature and corrosion, palladium-based thin wall tube membranes are used extensively as hydrogen-permeable membranes in many hydrogen-related reaction systems [28–30]. Khademi et al. proposed a novel reactor configuration for simultaneous methanol synthesis, cyclohexane dehydrogenation and hydrogen production [31,32]. In their study, methanol synthesis took place in the exothermic side and dehydrogenation of cyclohexane to benzene took place in the endothermic side. Also they used sweep gas flow across the permeate side for selective removal of permeated hydrogen through the Pd/Ag membrane. In other related work, Rahimpour and Bayat investigated the production of hydrogen by utilizing fluidization concept from the coupling of methanol and benzene synthesis in a hydrogen-permselective membrane reactor [33]. Their reported results indicated that combining reaction and

separation in a single catalytic membrane reactor leads to low energy consumption and smaller reactor length.

Only hydrogen molecules diffuse and other molecules are not small enough to pass through the small pores of the membrane. So the concentration of hydrogen decreases in the reaction zone and the reactions proceed to the right side. Pure hydrogen in the permeate side is collected and sent to SOFC as a feed. When pure hydrogen is used instead of other feeds, fuel cell performance enhances and there is no anode degradation. In this condition, only water is produced through the electrochemical reaction. The strongly exothermic electrochemical reaction increases the temperature of the cell. So for cooling the cell and preventing a temperature gradient across the cell, an excess air stream is used in the SOFC. The ionic conductivity of the oxygen ion conducting electrolyte enhances with increasing the temperature. So in this work, due to high operating temperature and also use of pure hydrogen as a feed of fuel cell, oxygen ion conducting electrolyte is superior to proton ion conducting electrolyte.

Recovery of flare gas for reusing in refineries prevents wasting a large amount of natural gas. Rahimpour et al. suggested three methods for purge gas recovery instead of conventional gas flaring [34,35]. These methods consist of Gas-to-Liquid (GTL) production technology, electricity generation with a gas turbine technique and compression and injection into refinery pipelines. The GTL plant includes three main steps involving, synthesis gas (syngas) production, Fisher–Tropsch synthesis and products upgrading. In this study, the recovery of purge gas to produce hydrogen as a feed of fuel cells will be considered as a new approach to reduce greenhouse gas emission.

2. Objective

Ammonia synthesis plant of Razi Petrochemical Complex is one of the main industrial plants to produce urea, nitric acid and ammonium nitrate in Iran. The purge gas which contains enormous quantities of co-produced gas and unreacted ammonia are flared as a waste byproduct. Owing to the environmental problems which are caused by ammonia and methane emission, the environmental regulations are intensely focused on controlling the purge gas emission to some allowable limits. The main goal of this study is investigating the purge gas recovery of ammonia synthesis plant by application of membrane reactor and SOFC technology as a new recovery approach. In this approach, ammonia and methane which exist in the purge gas of this plant are converted to hydrogen over nickel-based catalyst and then hydrogen permeates through Pd–Ag membrane reactor. In this configuration, the reactor walls are coated with a hydrogen perm-selective membrane to produce and separate pure hydrogen beside greenhouse gas elimination. Subsequently, the produced pure hydrogen is fed to an oxygen ion conducting electrolyte SOFC as a fuel to generate power.

This new approach, not only decreases greenhouse gas emission to the atmosphere, it uses ammonia synthesis purge gas as a source of hydrogen for generating the feed of fuel cells. In this work, the membrane reactor performance at different operating conditions will be studied and an electrochemical model will be developed to investigate the generated power in the SOFC.

3. Process description

The purge gas of ammonia plant and steam (steam to carbon ratio S/C is considered 2) is compressed and entered a double pipe catalytic membrane reactor. In the inner pipe which is called reaction side, the methane steam reforming and ammonia decomposition reactions occur simultaneously over Ni-based catalyst. A thin layer of Pd–Ag is covered the inner tube (reaction side) so that only hydrogen can permeate through it. Hydrogen which initially exists in the purge gas stream and also the produced hydrogen by the occurrence of reactions permeate through the Pd–Ag membrane to the shell side. A vacuum pump is used to increase the driving force in the shell side. Reducing the concentration of hydrogen in the tube side expedites the reactions to the right side. The pure hydrogen in the permeate side is collected and sent to the SOFC. Since steam is the only byproduct of SOFC, the required water for the reforming reactions in the membrane reactor can be supplied by recycling a portion of anode outlet gas [36]. A schematic diagram of proposed process is shown in Fig. 1.

The mathematical model will be developed based on the following assumptions:

- ✓ Steady state operation.
- ✓ Insulated SOFC.
- ✓ One dimensional flow.
- ✓ Ideal gas behavior of purge gas.
- ✓ Plug flow of the purge gas in the tube side.
- ✓ Isothermal operation of membrane reactor (The required heat for reactions can be supplied by a furnace across the reactor).
- ✓ Negligible pressure drop due to high operating pressure and relatively small reactor length.
- ✓ The ratio of steam to carbon is considered 2.

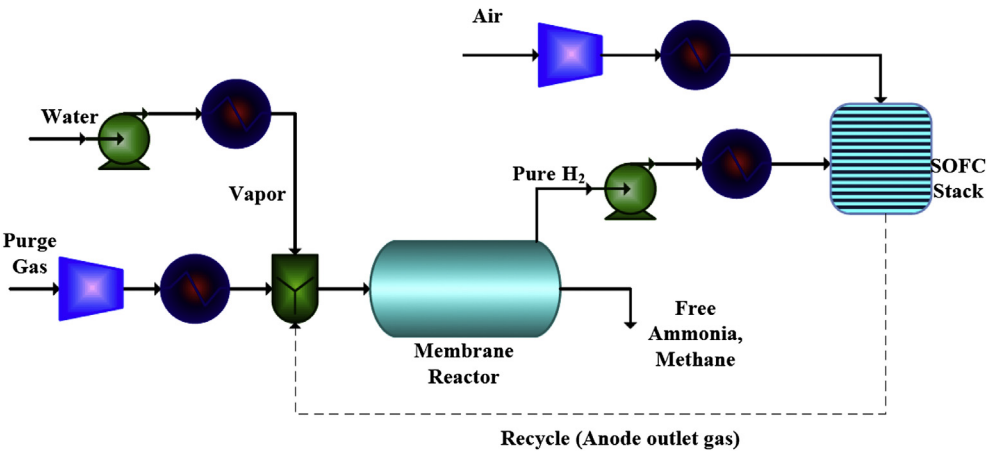

Fig. 1. Plant configuration of the integrated membrane reactor and SOFC.

Table 2
Kinetic parameters of reactions [25,42].

Reaction, j	Pre-exponential factor, $k_{0,i}$	Activation energy, E_i (kJ mol^{-1})
Ammonia decomposition	5.744×10^{19} (mol Pa$^{0.674}$ m^{-3} s^{-1})	230.4
Steam reforming	1.17×10^{15} (mol bar$^{0.5}$ kg cat^{-1} s^{-1})	240.1
Water gas-shift	5.43×10^{5} (mol kg cat^{-1} bar^{-1} s^{-1})	67.130
Overall steam reforming	2.83×10^{14} (mol bar$^{0.5}$ kg cat^{-1} s^{-1})	243.9

$k_i = k_{0,i} \exp(-E_i/RT)$.

3.1. Mathematical modeling of membrane reactor

3.1.1. Reaction side

The purge gas characteristics of the ammonia synthesis plant of Razi Petrochemical Complex are reported in Table 1 [37]. The purge gas stream and the required water enter the inner pipe of membrane reactor and reactions 2 to 5 occur over the Ni-based catalyst. At high hydrogen partial pressure, the rate of ammonia decomposition (reaction 2) can be described by Temkin–Phyzev mechanism [38].

$$r_{ad} = k_{ad}\left[\left(\frac{P_{NH_3}^2}{P_{H_2}^3}\right)^{\beta} - \frac{P_{N_2}}{K_{ad}^2}\left(\frac{P_{H_2}^3}{P_{NH_3}^2}\right)^{1-\beta}\right] \tag{6}$$

The first term in the bracket represents the decomposition rate and the second term refers to ammonia synthesis rate. The reported experimental value of β is about 0.674 [39]. Harrison and Kobe defined the thermodynamic equilibrium constant K_{ad} (Pa) as follows equation [40]:

$$\log\left(\frac{1}{K_{ad}}\right) = \frac{2250.322}{T} - 0.8534 - 1.51049l \times \log T - 25.8987 \times 10^{-5}T + 14.8961 \times 10^{-8}T^2 \tag{7}$$

The rates of methane steam reforming reactions (Eqs. (3)–(5)) are expressed as follows by Xu and Froment [41]:

Table 3
Van't Hoff parameters for species adsorption [42].

Species	$K_{0,k}$ (bar^{-1})	ΔH_k (kJ mol^{-1})
H_2	6.12×10^{-9}	−82.90
CH_4	6.65×10^{-4}	−38.28
CO	8.23×10^{-5}	−70.65
H_2O	1.77×10^{5}	88.68

$K_k = K_{0,k} \exp(-\Delta H_k/RT)$.

$$r_{SR} = \frac{k_{SR}}{P_{H_2}^{2.5}}\left(P_{CH_4}P_{H_2O} - \frac{P_{H_2}^3 P_{CO}}{K_{SR}}\right) \times \frac{1}{\phi^2} \tag{8}$$

$$r_{WGS} = \frac{k_{WGS}}{P_{H_2}}\left(P_{CO}P_{H_2O} - \frac{P_{H_2}P_{CO_2}}{K_{WGS}}\right) \times \frac{1}{\phi^2} \tag{9}$$

$$r_{Overall} = \frac{k_{Overall}}{P_{H_2}^{3.5}}\left(P_{CH_4}P_{H_2O}^2 - \frac{P_{H_2}^4 P_{CO}}{K_{Overall}}\right) \times \frac{1}{\phi^2} \tag{10}$$

where

$$\phi = 1 + K_{CO}P_{CO} + K_{H_2}P_{H_2} + K_{CH_4}P_{CH_4} + K_{H_2O}\frac{P_{H_2O}}{P_{H_2}} \tag{11}$$

The equilibrium constants of reactions are expressed as follows relations:

$$K_{SR} = \exp\left(\frac{-26,830}{T} + 30.114\right) \quad (\text{bar}^2) \tag{12}$$

$$K_{WGS} = \exp\left(\frac{4400}{T} - 4.036\right) \tag{13}$$

$$K_{Overall} = K_{SR} \times K_{WGS} \quad (\text{bar}^2) \tag{14}$$

The Arrhenius kinetic parameters for above reactions are listed in Table 2 [25,42]. Also the Van't Hoff parameters for species adsorption are represented in Table 3 [42].

3.1.2. Permeation side

The rate of hydrogen permeation through the thin layer of Pd–Ag membrane can be expressed as follows [43,44]:

$$J = \frac{J_0}{\delta}\exp\left(\frac{-E_p}{RT}\right) \times \left(P_{r,H_2}^{0.5} - P_{p,H_2}^{0.5}\right) \tag{15}$$

The value of pre-exponential factor (J_0) and activation energy (E_p) are taken as 3.2027×10^{-9} (mol cm cm^{-2} s^{-1} atm$^{-1/2}$) and 6.38 (kJ mol^{-1}), respectively [45,46]. P_r and P_p represent the partial pressure of H_2 at reaction side and permeation side, respectively. The permeation rate is inversely proportional to the thickness of the membrane layer (δ).

3.1.3. Mass and heat balance

A schematic diagram of catalytic membrane reactor is shown in Fig. 2. It is assumed that the reactor is divided into several small volumes and the finite difference method is employed. The mass balances for reaction and permeation sides are expressed as Eqs. (16) and (17), respectively.

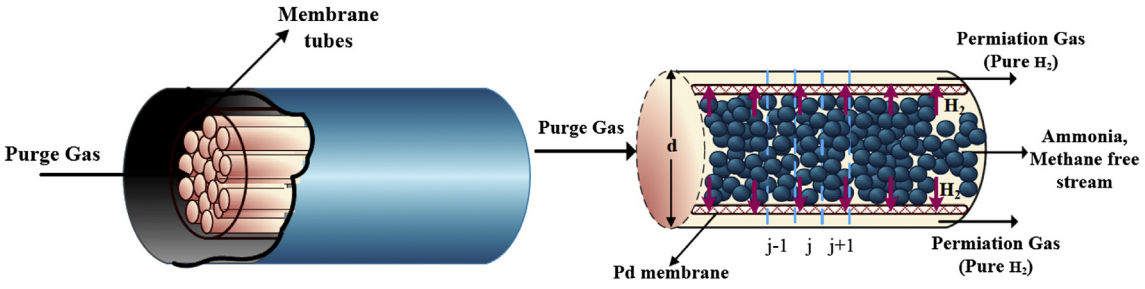

Fig. 2. A schematic of the membrane reactor.

Table 4
Input parameters for simulation of catalytic membrane reactor.

Pd–Ag film thickness, δ	6×10^{-6} (m)
Diameter of catalyst pellets	0.002 (m)
Catalyst density	510 (kg m^{-3})
Surface area of catalyst	190,000 (m^2 kg^{-1})
Void fraction	0.40
Flow rate of the purge gas	180 (mol h^{-1})
Steam to carbon ratio, *S/C*	2
Tube diameter, *d*	0.025 (m)
Tube length, *L*	3.50 (m)

$$f_{r,k}^{j+1} = f_{rk}^{j} + \frac{\rho_c \pi d^2 \Delta x}{4} \sum_i \nu_{ki} r_i^j - J_k^j \pi d \Delta x \tag{16}$$

$$f_{p,k}^{j+1} = f_{p,k}^{j} + J_k^j \pi d \Delta x \tag{17}$$

It is assumed that the membrane reactor operates at constant temperature. The required heat of endothermic reactions including methane steam reforming and ammonia decomposition are supplied by a furnace to maintain the temperature at a constant value across the length of the reactor. The necessary heat is calculated by summation of the reactions enthalpy as follows expression:

$$Q = \sum_i r_i \Delta H_i \tag{18}$$

where *i* refers to different reactions occur in the membrane reactor. The input parameters which are used for simulating the catalytic membrane reactor are summarized in Table 4.

Table 5
The activation over-potential data for Eq. (25) [52].

	k	*E*
Anode	6.54×10^{11} (Ω^{-1} m^{-2})	140 (kJ mol^{-1})
Cathode	2.35×10^{11} (Ω^{-1} m^{-2})	137 (kJ mol^{-1})

3.2. Mathematical modeling of SOFC

A steady state and planar model is developed to investigate the SOFC performance. Pure hydrogen from the permeate side of membrane reactor is fed to SOFC, so there is no internal steam reforming in SOFC. A schematic of the unit cell is shown in Fig. 3.

3.2.1. SOFC performance

The performance of SOFC is investigated by the following electrochemical model. The equilibrium potential or theoretical open circuit voltage can be expressed by the Nernst equation [47]:

$$E^{ner} = E^0 + \frac{RT}{2F} \ln\left(\frac{P_{H_2} P_{O_2}^{1/2}}{P_{H_2O}}\right) \tag{19}$$

where E^0 is the standard cell voltage at the standard pressure as a function of operating temperature and can be defined as the following equation [48]:

$$E^0 = 1.253 - 2.4516 \times 10^{-4} T \tag{20}$$

The second term on the right hand side of the Eq. (19) shows the effect of electrochemical reaction at the cell voltage. P_{H2} and P_{H2O} are the partial pressure of hydrogen and steam in the anode side at

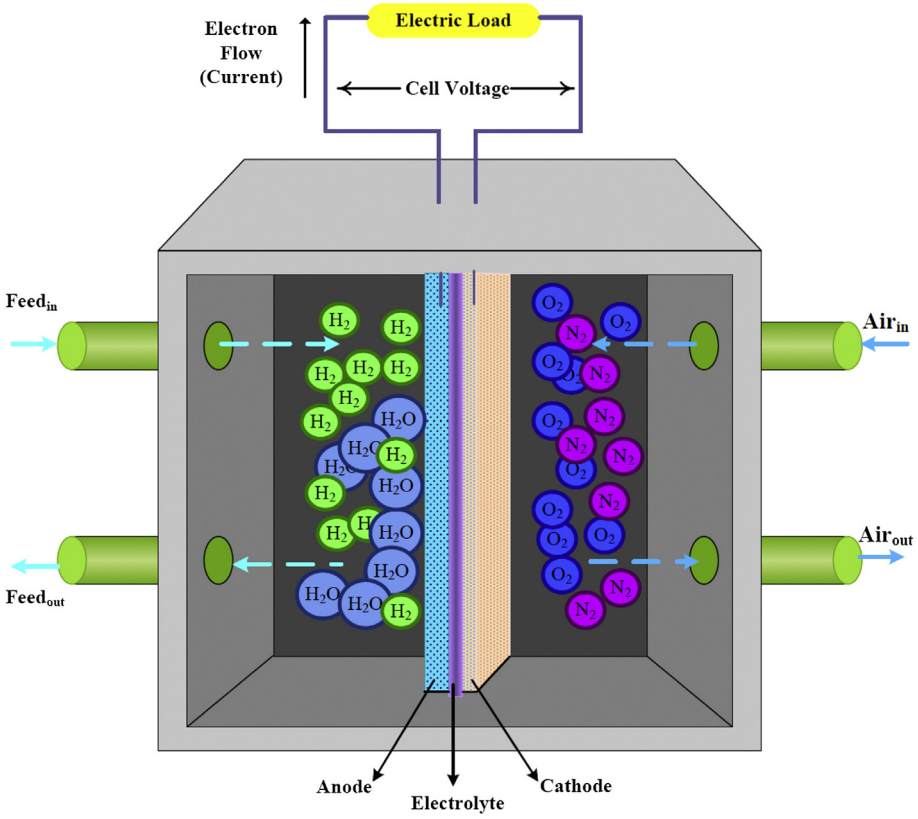

Fig. 3. A schematic of the SOFC.

Table 6
Input parameters for simulation of SOFC.

Property	Value
Cell area, A	0.02 (m^2)
Operating temperature, T	1073 (K)
Operating pressure, P	1 (bar)
Air composition, $x_{O_2}; x_{N_2}$	0.21; 0.79
Electrode porosity, ε_p [54]	0.3
Electrode tortuosity, ξ [54]	6
Electrode pore radius, r_p [54]	0.5 (μm)
Electrolyte conductivity [YSZ], σ_{elect} [55]	$3.34 \times 10^4 \exp(-10{,}300/T)(\Omega^{-1}\ m^{-1})$
Anode conductivity, σ_{an} [52]	8.0×10^4 ($\Omega^{-1}\ m^{-1}$)
Cathode conductivity, σ_{ca} [52]	8.4×10^3 ($\Omega^{-1}\ m^{-1}$)
Electrolyte thickness, τ_{elect}	10 (μm)
Anode thickness, τ_{an}	500 (μm)
Cathode thickness, τ_{ca}	50 (μm)

equilibrium state and P_{O2} refers to the partial pressure of oxygen in the cathode side.

In practice, the actual voltage of SOFC is less than the theoretical value due to several irreversible voltage losses including activation, concentration and ohmic over-potentials [49], so:

$$V = E^{ner} - \eta_{act} - \eta_{coc} - \eta_{ohm} \tag{21}$$

Ohmic losses occur due to ions transfer resistance through the electrolyte and electrons transfer resistance through the electrodes. Since the electrode resistance in the fuel cell is usually very small, it is considered negligible compared to the ionic resistance of the electrolyte. So the ohmic over-potential can be described by the Ohm's law [47].

$$\eta_{ohm} = j\Re_{ohm} \tag{22}$$

where

$$\Re_{ohm} = \frac{\tau_{anode}}{\sigma_{anode}} + \frac{\tau_{electrolyte}}{\sigma_{electrolyte}} + \frac{\tau_{cathode}}{\sigma_{cathode}} \tag{23}$$

The activation loss is the voltage drop that associated with the electrochemical reactions occurring at the electrode–electrolyte interfaces and can be expressed by the following equation [50]:

$$\eta_{act} = \frac{RT}{F}\sinh^{-1}\left(\frac{j}{2j_{0,anode}}\right) + \frac{RT}{F}\sinh^{-1}\left(\frac{j}{2j_{0,cathode}}\right) \tag{24}$$

Table 7
The parameters used for comparison between membrane reactor of model and Gobina results [24].

Volume of the catalyst bed	6.689×10^{-6} (m^3)
Pd–Ag film thickness, δ	6×10^{-6} (m)
Diameter of catalyst pellets	0.0015–0.002 (m)
Catalyst density	510 (kg m^{-3})
Surface area of catalyst	190,000 ($m^2\ kg^{-1}$)
Void fraction	0.4
Pressure of synthesis gas	36 (atm)
Pressure of sweep gas steam	1 (atm)
Flow rate of synthesis gas	350 ($cm^3\ min^{-1}$)
Flow rate of sweep gas steam	300 ($cm^3\ min^{-1}$)
Tube length	0.14 (m)
Feed composition	(mol %)
H_2	20
NH_3	0.3
N_2	48
H_2O	1.5
CH_4	4.2
$CO + CO_2$	26

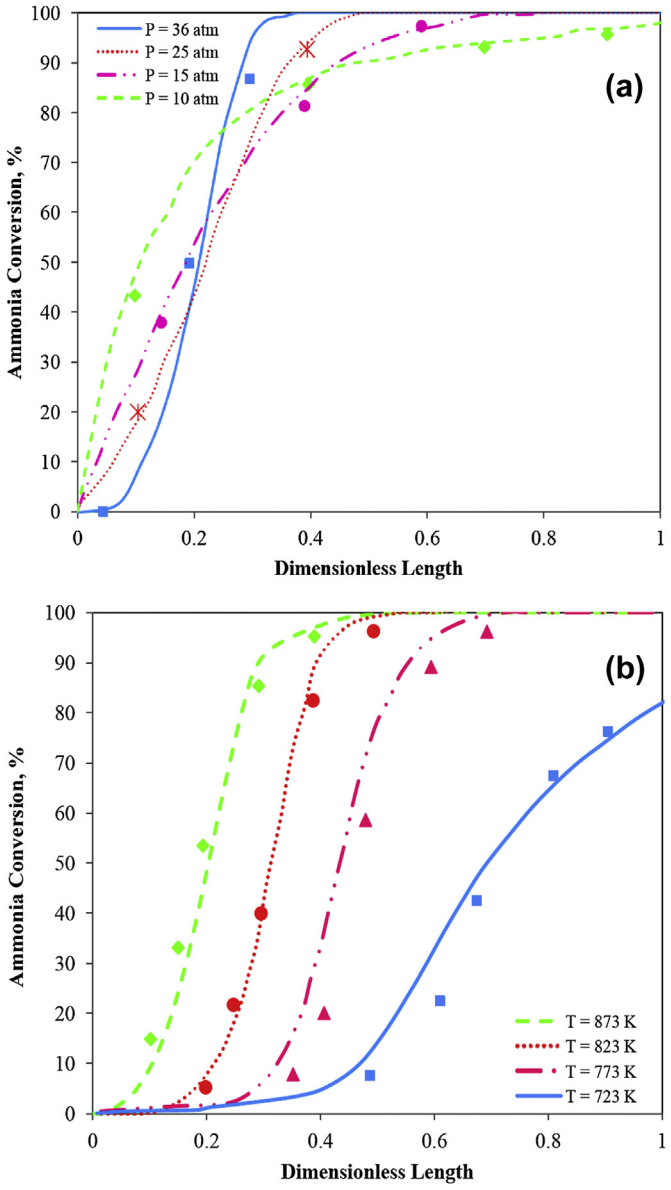

Fig. 4. Comparison of ammonia decomposition between model and Gobina et al. results [24]: (a) different pressure, (b) different temperature.

$j_{0,electrode}$ is the exchange current density and its value is highly influenced by the electrode material, structure, temperature of the reaction and the length of triple-phase boundary (TPB) [51]. It is normally expressed as:

$$j_{0,electrode} = \frac{RT}{nF} k_{electrode} \exp\left(\frac{-E_{electrode}}{RT}\right) \tag{25}$$

The values of $k_{electrode}$ and $E_{electrode}$ are reported in Table 5 [52].

Concentration over-potential is created by concentration variation of fuel and oxygen at the electrode–electrolyte interfaces due to mass transport phenomena.

$$\eta_{conc,anode} = \frac{RT}{2F}\ln\left[\frac{P^I_{H_2O}(an)P_{H_2}(an)}{P_{H_2O}(an)P^I_{H_2}(an)}\right] \tag{26}$$

$$\eta_{con,cathode} = \frac{RT}{4F}\ln\left[\frac{P_{O_2}(ca)}{P^I_{O_2}(ca)}\right] \tag{27}$$

Table 8
Comparison of ammonia conversion modeling results with experimental data reported by Gobina et al. [24].

(a) At different pressures				
Pressure (atm)	Dimensionless length	Experimental data %	Modeling conversion %	Absolute error %
$P = 36$	0.05	0	1.4	1.4
	0.20	50	45	5
	0.30	87	94	7
$P = 25$	0.10	20	19	1
	0.40	93	95	2
$P = 15$	0.14	38	41	3
	0.40	81	84	3
	0.60	97	96	1
$P = 10$	0.10	43	45	2
	0.40	86	87	1
	0.70	93	94	1
	0.90	96	97	1
(b) At different temperatures				
Temperature (K)	Dimensionless length	Experimental data %	Modeling conversion %	Absolute error %
$T = 873$	0.10	15	10	5
	0.15	33	29	4
	0.20	53	51	2
	0.30	85	93	8
	0.40	95	97	2
$T = 823$	0.20	5	9	4
	0.25	22	21	1
	0.30	40	44	4
	0.40	82	93	11
	0.50	96	99	3
$T = 773$	0.35	8	16	8
	0.40	20	33	13
	0.50	58	69	11
	0.60	89	94	5
	0.70	96	99	3
$T = 723$	0.50	8	16	8
	0.60	22	35	13
	0.70	43	50	7
	0.80	67	63	4
	0.90	76	74	2

$P^I_{H_2}$, $P^I_{H_2O}$ and $P^I_{O_2}$ are the partial pressure of hydrogen, steam and oxygen at the electrode–electrolyte interfaces, respectively. According to the Fick's model, the electrochemical reaction occurs at the electrode–electrolyte interfaces. So the diffusion rate of

Table 9
The parameters used for comparison between the present SOFC model and Rogers results [56].

Operating temperature, T	1073 (K)
Operating pressure, P	1 (bar)
Air composition, $x_{O_2}; x_{N_2}$	0.21; 0.79
Fuel composition, $x_{H_2}; x_{H_2O}$	0.95; 0.05
Electrode porosity, ϵ_p	0.38
Electrode tortuosity, ξ [57]	2.75
Electrode pore radius, r_p [58]	0.75 (μm)
Electrolyte conductivity [YSZ], σ_{elect}	0.64 (Ω^{-1} m^{-1})
Anode conductivity, σ_{an}	71,429 (Ω^{-1} m^{-1})
Cathode conductivity, σ_{ca}	5376 (Ω^{-1} m^{-1})
Electrolyte thickness, τ_{elect}	10 (μm)
Anode thickness, τ_{an}	1000 (μm)
Cathode thickness, τ_{ca}	50 (μm)
Anode reaction zone layer thickness	20 (μm)
Cathode reaction zone layer thickness	20 (μm)
Reference H_2 concentration, c_{H_2}	10.78 (mol m^{-3})
Reference O_2 concentration, c_{O_2}	2.38 (mol m^{-3})
Reaction order for H_2 oxidation	0.5
Reaction order for O_2 oxidation	0.5

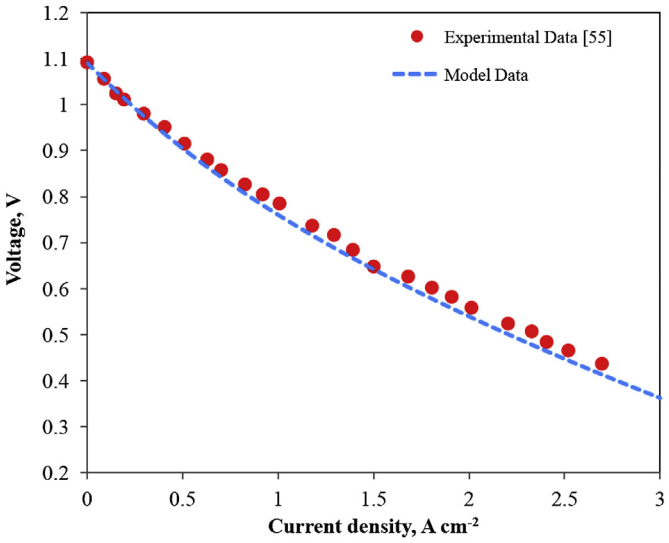

Fig. 5. Comparison of the cell performance between model and Rogers results [56].

reactants to the interface is equal to the rate of electrochemical reaction [53].

$$P^I_{H_2}(an) = P_{H_2}(an) - \frac{RT\tau_{an}}{2FD_{eff,an}}j \tag{28}$$

$$P^I_{H_2O}(an) = P_{H_2O}(an) + \frac{RT\tau_{an}}{2FD_{eff,an}}j \tag{29}$$

$$P^I_{O_2}(ca) = P - (P - P_{O_2}(ca))\exp\left(\frac{RT\tau_{ca}}{4FD_{eff,ca}P}j\right) \tag{30}$$

For equimolar counter-current mass transfer, the anode effective diffusion coefficient is expressed as [54]:

$$D_{eff,an} = \left(\frac{P_{H_2}}{P_{an}}\right)D_{H_2O(eff)} + \left(\frac{P_{H_2O}}{P_{an}}\right)D_{H_2(eff)} \tag{31}$$

The effective diffusion coefficient for the cathode represents the oxygen effective diffusivity coefficient in a binary gas mixture of N_2 and O_2 and is expressed as:

$$D_{eff,ca} = D_{O_2(eff)} \tag{32}$$

where,

$$\frac{1}{D_{k(eff)}} = \frac{\xi}{\varepsilon}\left(\frac{1}{D_{bulk,k}} + \frac{1}{D_{knudsen,k}}\right) \tag{33}$$

Table 10
Comparison of SOFC modeling results with experimental data reported by Rogers [56].

Current density (A cm^{-2})	Experimental data (V)	Modeling data (V)	Mean error %
0.5	0.91	0.90	1.0
1.0	0.78	0.76	2.5
1.5	0.65	0.64	1.5
2.0	0.56	0.54	3.6
2.5	0.47	0.45	4.2

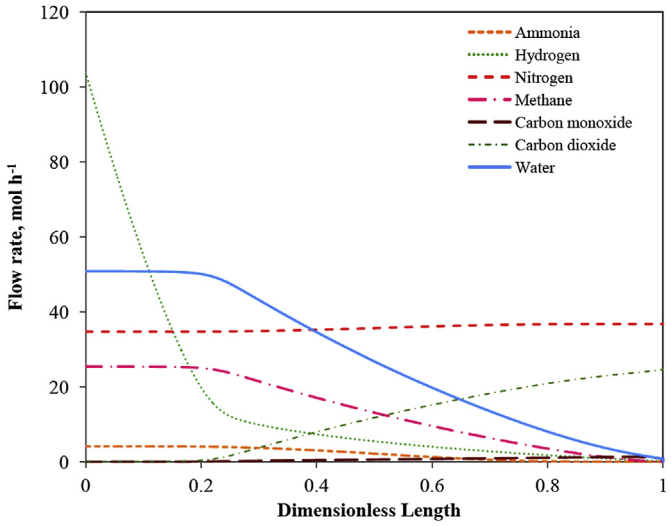

Fig. 6. Species flow rates in the membrane reactor at 873 K and 35 bar.

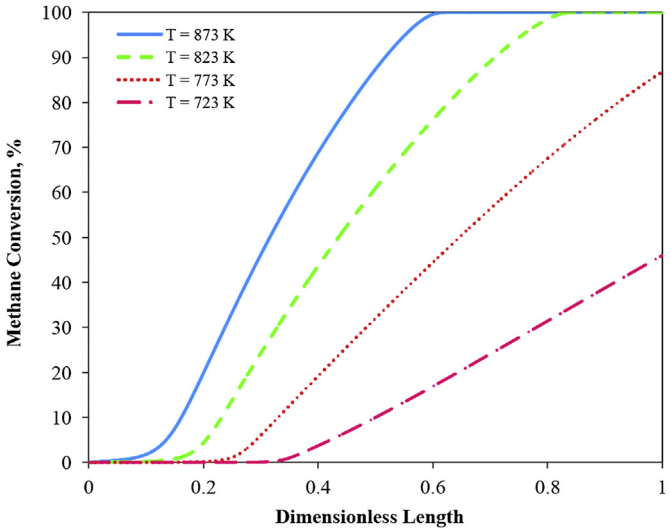

Fig. 8. Effect of tube side temperature on the methane conversion at 35 bar.

SOFC efficiency represents the fraction of the total chemical energy of the inlet feed converted to electrical energy. The output power and electrical efficiency of the cell are calculated as:

$$\dot{P}_{SOFC} = j \cdot A \cdot V \tag{34}$$

$$\varepsilon_{SOFC} = \frac{P_{SOFC}}{LHV \times f^0_{fuel}} \tag{35}$$

As represented in Eq. (35), the efficiency is inversely proportional to the inlet flow rate of the feed. By considering a constant value for fuel utilization which is defined as the fraction of the hydrogen that is consumed in the cell, the flow rate of the feed can be calculated as follows.

$$f^0_{fuel} = \frac{j \times A}{2Fy^0_{H_2} U_{fuel}} \tag{36}$$

The input parameters for simulation of SOFC are listed in Table 6. A typical SOFC electrolyte is yttria-stabilized zirconia (YSZ), an oxide ion conductor at elevated temperatures. The anode is usually a nickel/zirconia cermet, which provides appropriate chemical stability, low cost and high electrochemical performance, and the cathode is a perovskite material, such as strontium doped lanthanum manganite, often mixed with YSZ in the form of a composite.

4. Model validation

4.1. Catalytic membrane reactor validation

Gobina et al. examined the removal of ammonia in the gasification of coal process using a Pd–Ag membrane reactor [24]. To confirm the modeling results, a comparison is made between modeling result and reported data by Gobina et al. [24]. The comparison is carried out based on the data listed in Table 7. Fig. 4(a) and (b) represents the conversion of ammonia through the length of reactor at different temperature and pressure. The specified points in the figures show the experimental results. As shown in

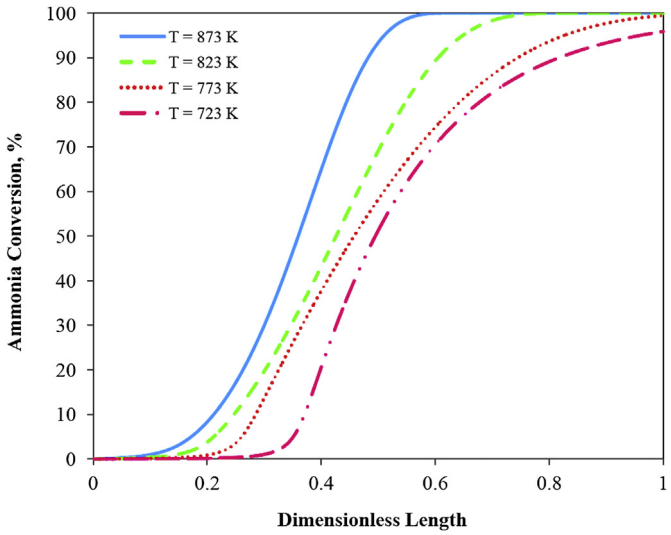

Fig. 7. Effect of tube side temperature on the ammonia conversion at 35 bar.

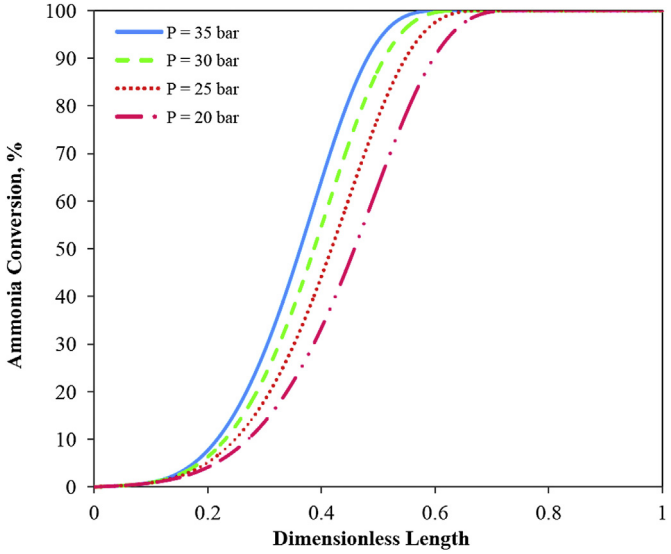

Fig. 9. Effect of tube side pressure on the ammonia conversion at 873 K.

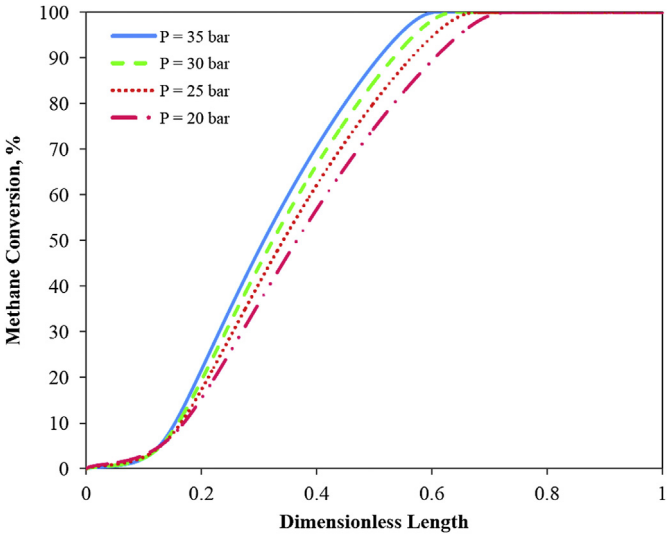

Fig. 10. Effect of tube side pressure on the methane conversion at 873 K.

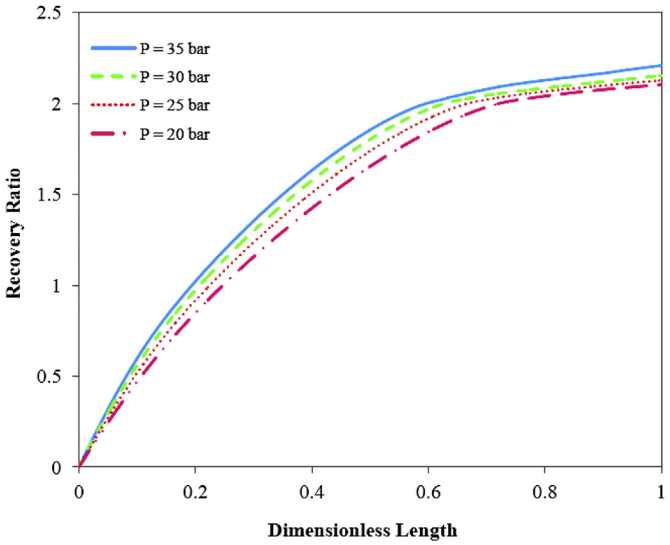

Fig. 12. Effect of tube side pressure on the recovery ratio at 873 K.

this figure and based on absolute errors reported in Table 8, the modeling results satisfy the experimental data, appropriately. There is an insignificant error for ammonia conversion along the reactor tube length over the pressure range 10–36 atm and temperature range 723–873 K.

4.2. Solid oxide fuel cell validation

The SOFC modeling results are validated using the reported data by Rogers et al. [56]. The cell is supplied with 95% H_2 and 5% H_2O. The input parameters used for model validation of the SCFC are represented in Table 9. All the parameters considered in the model validation are obtained from Rogers et al. study except the parameters which are referenced. Fig. 5 shows the variation of generated voltage via current density. The represented relative errors in Table 10 show that the model predicted results have a good agreement with the experimental results reported by Rogers et al. [56]. As indicated in this figure, the generated voltage decreases continuously with increasing the current density.

5. Results and discussion

In the following sections, the performance of proposed configuration for purge gas recovery of ammonia synthesis plant will be considered with more details. In the first part, the effect of some related parameters including tube side temperature and pressure on the ammonia decomposition and methane steam reforming reactions in the catalytic membrane reactor are considered. Also for more investigation, the amount of recovered hydrogen along the reactor length with different tube numbers is evaluated. In the second part, the performance of the SOFC is investigated by evaluating the actual voltage and generated power in the various conditions. Eventually, the power that can be generated by the ammonia synthesis plant purge gas in an integrated catalytic membrane reactor and SOFC system, and also the numbers of required cells are calculated. The effect of recycling the anode outlet gas of SOFC (high water content) to the catalytic membrane reactor for supplying the required water is considered.

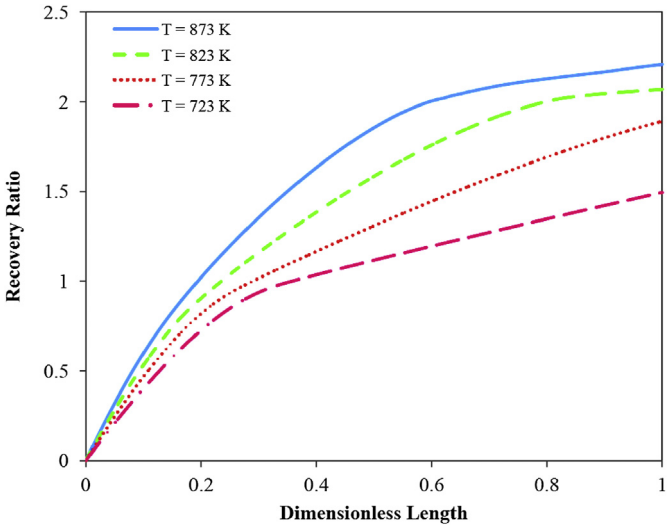

Fig. 11. Effect of tube side temperature on the recovery ratio in 35 bar.

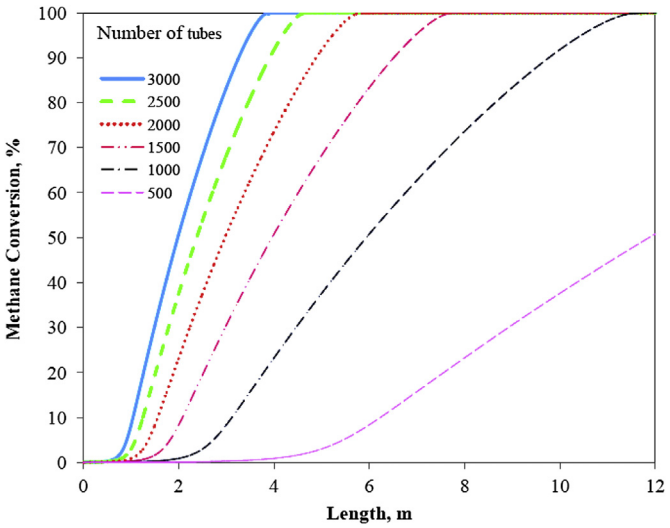

Fig. 13. Methane conversion along the reactor length by various tube numbers.

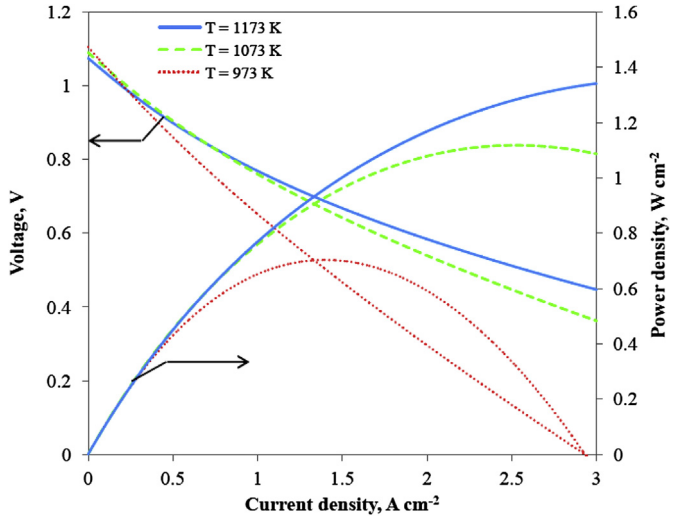

Fig. 14. Actual voltage and power density as a function of current density at different temperatures.

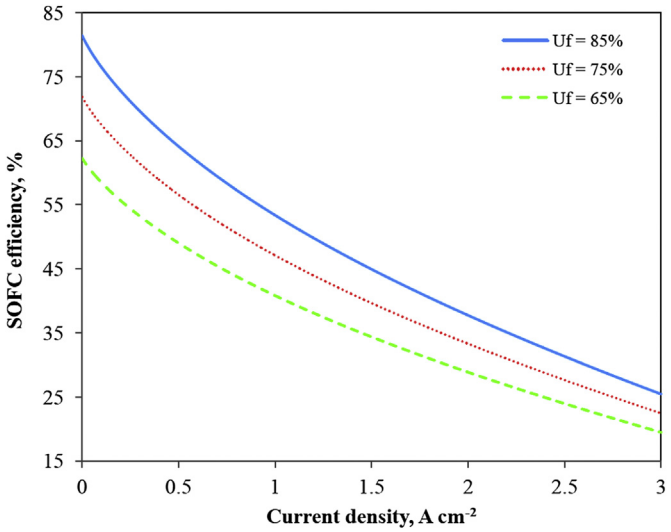

Fig. 16. Effect of fuel utilization on the SOFC efficiency.

5.1. Performance investigation of the catalytic membrane reactor

Fig. 6 shows the variation of different species flow rates in the membrane reactor at 873 K and 35 bar while S/C is 2. It is clear that at the beginning of the membrane reactor, since the concentration of hydrogen is high, hydrogen permeates rapidly but the rate of steam reforming and ammonia decomposition reactions are slow. While the concentration of hydrogen decreases, the rate of reactions increase and the concentration of methane and ammonia decrease. Nitrogen is slightly produced in the ammonia decomposition reaction so its flow rate increases. The flow rates of carbon monoxide and carbon dioxide increase with increasing the rate of methane steam reforming and water gas-shift reactions. Also the flow rate of water decreases by increasing the rate of the reactions. Therefore at the end of the membrane reactor, ammonia decomposition and methane conversion to carbon monoxide and carbon dioxide take place completely. There is a slight amount of carbon monoxide in the outlet stream and hydrogen permeates completely through the membrane.

5.1.1. Effect of tube side temperature

Figs. 7 and 8 show the effect of tube side temperature on the ammonia decomposition and methane steam reforming reactions along the membrane reactor length, respectively. At the entrance of the tube, since the concentration of hydrogen is high, the conversion of ammonia and methane will not occur until a part of initial hydrogen permeates. As temperature increases, the rate of the reactions and hydrogen permeation increase, so the conversion of methane and ammonia enhance. The ammonia decomposition and methane steam reactions complete at the shorter length of the reactor. The required reactor length to reach the complete conversion of reactants at higher temperatures such as 873 K is shorter than the ones for the lower temperatures. As indicated in Fig. 7, for temperature below 773 K, the ammonia conversion is not 100% along the length of the reactor and the tube must be longer. As shown in Fig. 8, the methane converts completely at temperature above 800 K. Increasing the temperature, enhances the rate of reactions, so more hydrogen is produced through the reactions. Increasing the hydrogen concentration enhances the driving force

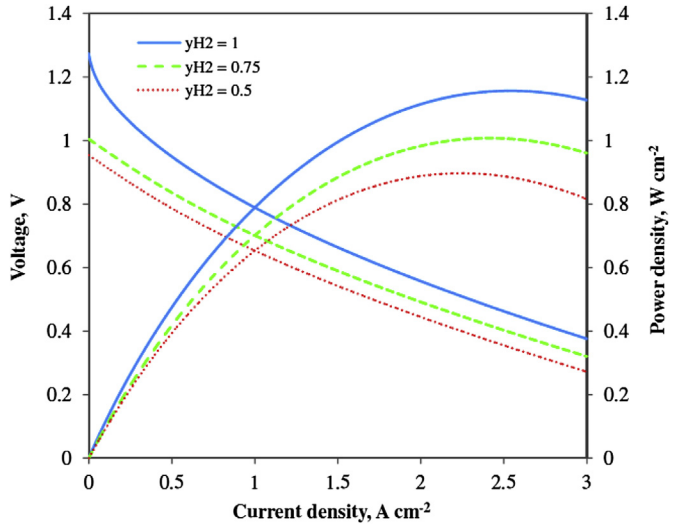

Fig. 15. Actual voltage and power density as a function of current density at different hydrogen concentrations.

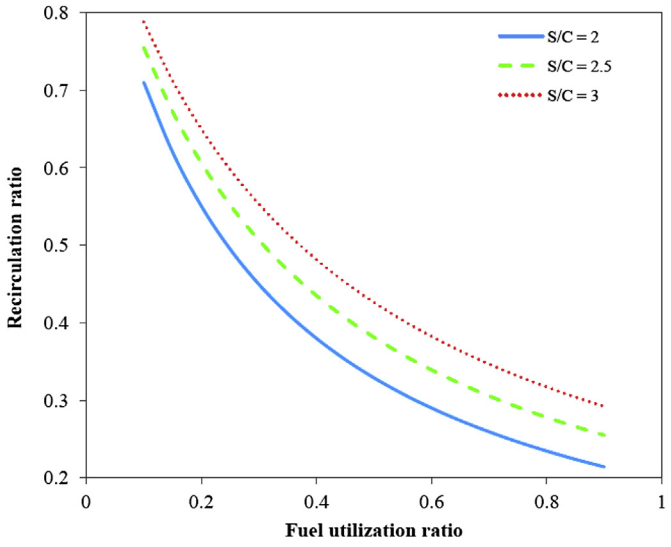

Fig. 17. Recirculation ratio as a function of fuel utilization in different S/C.

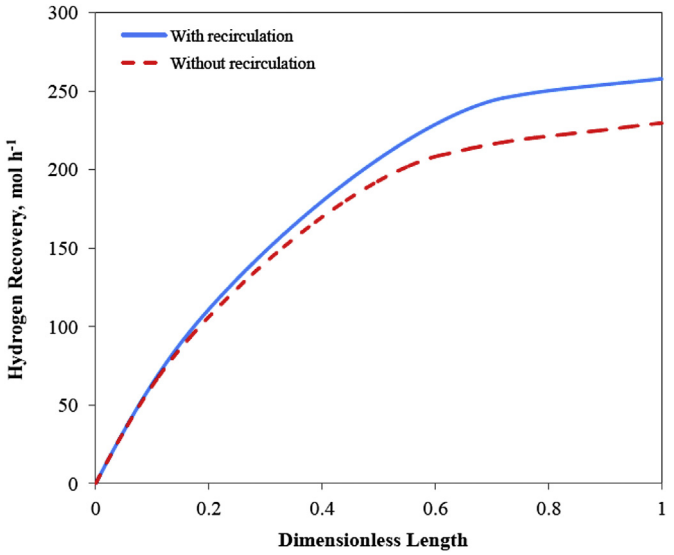

Fig. 18. Effect of recirculation on recovered hydrogen along the reactor length.

and causes more hydrogen permeation and as a result, the equilibrium of the reactions shifts to the right. Hence the reactor has a better performance at high temperature.

5.1.2. Effect of tube side pressure

Figs. 9 and 10 show the effect of tube side pressure on the ammonia conversion and methane reforming along the tube length, respectively. According to the Le Chaterlier's principle, increasing the tube side pressure shifts the equilibrium of the steam reforming reaction and ammonia decomposition to the left side. But as shown in Figs. 9 and 10, increasing the pressure has a positive effect on the reactant conversion in the membrane reactor due to increasing the rate of hydrogen permeation and as a result increasing the driving forces. As indicated in Fig. 9, at higher pressure, ammonia is decomposed faster and the required length of tube for complete conversion is shorter. Also as shown in Fig. 10, the pressure of the tube side has the same effect on the methane conversion. So ammonia and methane conversions reach to 100% at 873 K and the pressure range of 20–35 bar. Hence, in a catalytic membrane reactor, increasing the tube side pressure improves the reactor performance.

5.1.3. Recovery ratio

Recovery is defined as the ratio of the permeated hydrogen to the initial flow rate of hydrogen in the feed. Since hydrogen produces through the reactions, the hydrogen recovery ratio increases through the length of the reactor. Figs. 11 and 12 indicate the recovery ratio at different operating conditions. Because of hydrogen production through the ammonia decomposition and methane steam reforming reactions, the increasing rate of recovery ratio is high, but through the length of the reactor, due to decreasing the hydrogen production, this ratio tends to a certain value. According to Fig. 11, increasing the tube side temperature enhances the recovery ratio because of increasing the permeation rate of hydrogen. The maximum recovery ratio at 723, 773, 823 and 873 K is 1.5, 1.9, 2 and 2.2, respectively. Since the methane and ammonia conversion reaches to a certain value in the pressure range of 20–35 bar, so the amount of produced hydrogen is constant. Therefore as represented in Fig. 12, although increasing the operating pressure improves the hydrogen permeation, it has not significant effect on the recovery ratio and in all cases, this ratio reaches to a certain value.

5.1.4. Effect of tube numbers

Due to reactor design limitations, the size of the reactor is one of the most important decision parameters. It is clear that to reach complete reactant conversion, a specific contact area is necessary, and so the length of the reactor can be decreased by increasing the tube numbers in the membrane reactor. Fig. 13 shows the methane conversion through the length of the reactor with different tube numbers. As indicated in this figure, with decreasing the tube numbers from 3000 to 1500, the required reactor length to reach complete methane conversion should be increased from 4 to 8 m. The total purge gas of ammonia synthesis plant in the Razi petrochemical complex is 570 kg mol h^{-1}. Based on the reported parameters in Table 4, the required tube numbers to reach complete conversion of ammonia and methane at 873 K and 35 bar is about 3160, where the length of the reactor is 3.5 m.

5.2. SOFC performance

5.2.1. Effect of operating temperature

The SOFC performance will be considered by evaluating the generated power, actual voltage and electrical efficiency. According to Eqs. (22)–(27), increasing current density enhances the over potentials and decreases the actual voltage. So as indicated in Fig. 14, the actual voltage versus current density curve has a descending trend. But the power density has a parabolic trend with increasing current density which is related to the power definition. By increasing the current density, the power density enhances to reach a maximum point. Then, the effect of decreasing the actual voltage overcomes the effect of current density enhancement and as a result the generated power will decrease. Also the effect of operating temperature on the actual voltage and generated power is investigated in this figure. Temperature enhancement leads to increase the conductivity of electrolyte, thus the ohmic overpotential decreases and actual voltage and generated power increase. According to this figure, with the increasing temperature, the actual voltage and power density increase due to higher conductivity of the electrolyte at elevated temperatures. Based on the presenting conditions in Table 6, the maximum power density at 973, 1073 and 1173 K is 0.7, 1.1 and 1.36 W cm^{-2}, respectively.

5.2.2. Effect of feed composition

The performance of the cell is strongly affected by the concentration of hydrogen in the feed. Fig. 15 shows the actual voltage and power density in the various compositions of hydrogen. According to this figure, in the feed with more hydrogen content, the E^{ner} has a higher value. Increasing the concentration of hydrogen in the feed will be decreasing the concentration over-potential of anode. Therefore the actual voltage and power density enhance by increasing the hydrogen concentration. The maximum power density is 1.15 W cm^{-2} when the pure hydrogen is used as a feed, but it is about 1 and 0.89 W cm^{-2} when hydrogen composition is 0.75 and 0.25, respectively. It is obvious that the pure hydrogen has the best operation in the cell. So the hydrogen selective membrane reactor generates the best quality of the feed for SOFC.

5.2.3. SOFC efficiency at different fuel utilization ratio

According to efficiency definition (Eq. (35)), it is inversely proportional to feed flow rate. Also based on Eq. (36), the flow rate is inversely proportional to fuel utilization ratio. So it is obvious that, the SOFC has a greater efficiency at a higher fuel utilization ratio due to its lower feed flow rate. This fact is shown in Fig. 16. Also this figure indicates a descending trend for the efficiency versus the current density curve. Enhancement of the current density increases the molar flow rate of the feed and so the SOFC efficiency decreases. As represented in this figure, at 1.5 A cm^{-2}, when the fuel

utilization ratio decreases from 85% to 75% and 65%, the SOFC efficiency decreases from 44.9 to 39.6 and 34.3, respectively.

5.2.4. Total generated power

The total generated power in the SOFC is related to the number of cells and can be calculated according to Eq. (37).

$$P^{t}_{SOFC} = P_{SOFC} \times N_{cell} \quad (37)$$

The number of required cells depends on the molar flow rate of the feed sent to SOFC system. In this study, the inlet feed of SOFC system is pure hydrogen which is generated in the membrane reactor. Therefore the molar flow rate of the feed of SOFC system is related to the operating conditions of catalytic membrane reactor. If the total generated hydrogen in the reactor is sent to SOFC, the number of cells calculates by dividing the total amount of recovered hydrogen to the inlet flow rate of the SOFC. So according to the simulation conditions presented in Tables 4 and 6, when the tube side temperature and pressure of the membrane reactor are so high, for recovery of all hydrogen at a fuel utilization 0.75, about 11 cells per a tube of membrane reactor are required. While pure hydrogen is used as a feed of SOFC, the maximum power density for any cell is 1.15 W cm^{-2}. In an integrated catalytic membrane reactor and SOFC system using the purge gas of ammonia synthesis plant as the feed, about 8 MW power can be generated as well as removing the ammonia and methane from the purge gas.

5.2.5. Effect of recirculation ratio

Anode outlet gas contains high water vapor content. So the required water for the steam reforming reaction in the membrane reactor can be supplied by recycling a portion of anode outlet gas. The amount of recycling depends on the S/C ratio in the membrane reactor. For the greater S/C ratio, more water content must be supplied, so the recirculation ratio should be higher to adjust the S/C ratio on a fix value. According to Fig. 17, at higher fuel utilization ratio, more hydrogen participates in the electrochemical reaction, and as a result, more water produces the cells as a byproduct. So the recirculation ratio for providing the required water of reforming reaction in the membrane reactor will decrease.

The effect of recycling the anode outlet gas on the hydrogen recovery in the membrane reactor is shown in Fig. 18. As indicated, when the required water is supplied by recycling a portion of anode outlet gas, the amount of recovered hydrogen increases, because the recycled stream contains an amount of hydrogen that is not consumed in the fuel cell. So the hydrogen percentage in the feed of membrane reactor increases and as a result more hydrogen will be recovered.

6. Conclusions

In order to recover the purge gas of ammonia synthesis plant, an integrated configuration of catalytic hydrogen-permselective membrane reactor and solid oxide fuel cell (SOFC) system have been investigated. In this new approach, ammonia and methane as the main greenhouse gases in the purge gas are converted to pure hydrogen through methane steam reforming and ammonia decomposition reactions over nickel-based catalyst in the membrane reactor. The produced hydrogen permeates through Pd–Ag membrane and it is sent to the SOFC as a feed. The modeling results illustrate that increasing temperature and pressure of the reactor enhances the conversion of methane and ammonia so that it reaches to 100% at 873 K and 35 bar through 0.6 length of the reactor. Furthermore increasing the operating temperature enhances the recovery ratio of hydrogen by increasing permeation rate, while increasing the operating pressure has not significant effect on it. The required tube numbers to recover the total amount of purge gas stream of ammonia synthesis plant in the Razi petrochemical complex at 873 K and 35 bar is about 3160. Also parametric analysis of SOFC shows that the cell has better performance in higher temperature, hydrogen composition and fuel utilization. By recycling a portion of anode outlet stream to the membrane reactor not only the required water for steam reforming reaction is supplied, the amount of recovered hydrogen increases. By applying this new configuration, about 8 MW power is generated by recovery of the purging gas stream of ammonia synthesis plant in the Razi petrochemical complex.

Acknowledgment

The authors gratefully acknowledge the financial support for this work that was provided by Renewable Energy Organization of Iran.

Nomenclature

A	active surface area, m^2
D	tube diameter, m
D_{eff}	effective diffusion coefficient, $m^2\ s^{-1}$
$E_{electrode}$	activation energy of the exchange current density, kJ mol^{-1}
E_i	activation energy for i-th reaction, kJ mol^{-1}
E_p	activation energy for hydrogen permeation, kJ mol^{-1}
E^{ner}	Nernst voltage, V
E^0	open circuit voltage at the standard pressure, V
F	Faraday constant, C mol^{-1}
F	molar flow rate
J_k	permeation rate of component k, mol s^{-1}
J_0	permeation rate constant, mol cm $cm^{-2}\ s^{-1}\ atm^{-1/2}$
J	current density, A m^{-2}
$j_{0,e;ectrode}$	exchange current density, A m^{-2}
$k_{electrode}$	pre-exponential factor of exchange current density, A m^{-2}
k_i	reaction rate constant for i-th reaction
K_i	equilibrium constant for i-th reaction
K_k	adsorption constant for component k
L	cell length, m
L	axial position in reactor, m
LHV	lower heating value
N	number of electrons participating in the electrochemical reaction
N_{cell}	number of cells
P	pressure, bar
P_k	partial pressure of component k, bar
P^l_k	partial pressure of component k in the electrode electrolyte interface, bar
P_{SOFC}	power density, W m^{-2}
Q	required heat for reactions, J s^{-1}
R	universal gas constant, J $mol^{-1}\ K^{-1}$
r_i	rate of reaction i
$\Re_{ohm}$	total cell resistance, $\Omega\ m^2$
r_p	pore radius, m
T	temperature, K
U_f	fuel utilization ratio
V	actual voltage, V
y^0_k	molar fraction of component k at inlet

Greek letters

B	exponential constant in the rate of ammonia decomposition
Δ	membrane thickness, m
ΔH_k	heat of absorption for component k, J mol^{-1}

E	electrode porosity
ε_{SOFC}	solid oxide fuel cell efficiency
H	over-potential loss, V
$\nu_{k,i}$	stoichiometric coefficient of component k in reaction i
Ξ	electrode tortuosity
P	density, kg m^{-3}
σ_{anode}, $\sigma_{cathode}$	electronic conductivity of the anode and cathode, Ω^{-1} m^{-1}
$\sigma_{electrolyte}$	ionic conductivity of the electrolyte, Ω^{-1} m^{-1}
T	thickness, m

Superscripts

I	interface of electrode electrolyte
J	j-th control volume
T	total

Subscripts

Act	activation
Ad	ammonia decomposition
An	anode
Ca	cathode
Con	concentration
Elect	electrochemical reaction
F	fuel
I	reaction
K	component
P	permeation side
Ohm	ohmic
R	reaction side
SR	steam reforming
WGS	water gas-shift

References

[1] M.R. Rahimpour, K. Alizadehhesari, Int. J. Hydrogen Energy 34 (2009) 1349–1362.
[2] C.J. Winter, Int. J. Hydrogen Energy 31 (2006) 1623–1631.
[3] L. Petruzzi, S. Cocchi, F. Fineschi, J. Power Sources 118 (2003) 96–107.
[4] F. Arpino, N. Massarotti, Energy 34 (2009) 2033–2041.
[5] U.S. Department of Energy/Morgantown Energy Technology Center, Program Research and Development Announcement for: Advanced Concepts in Ceramic Membranes for High Temperature Gas Separation, RFP No. DE-RA21-89MC26038, December, 1988.
[6] J. Shu, B.P.A. Grandjean, S. Kaliaguine, Appl. Catal. A Gen. 119 (1994) 302–325.
[7] F. Gallucci, A. Basile, Int. J. Hydrogen Energy 33 (2008) 1671–1687.
[8] Y. Lin, S. Liu, C. Chuang, Y. Chu, Catal. Today 82 (2003) 127–139.
[9] F. Gallucci, L. Paturzo, A. Fama, A. Basile, Ind. Eng. Chem. Res. 43 (2004) 928–933.
[10] G. Manzolini, S. Tosti, Int. J. Hydrogen Energy 33 (2008) 5571–5582.
[11] D. Saebea, S. Authayanun, Y. Patcharavorachot, W. Paengjuntuek, A. Arpornwichanop, Energy 51 (2013) 1068–1075.
[12] H. Takenaka, E. Torikai, Y. Kawami, Int. J. Hydrogen Energy 7 (1982) 397–403.
[13] S.A. Topham, The history of the catalytic synthesis of ammonia, in: J.R. Anderson, M. Boudart (Eds.), Catalysis Science and Technology, Springer-Verlag, Berlin-Heidelberg, 1985, pp. 1–50.
[14] T. Asami, M. Tanakat, Y. Yanagisawa, Cryogenics 36 (1996) 997–1003.
[15] Q.L. Ma, R.R. Peng, L.Z. Tian, G.Y. Meng, Electrochem Commun. 8 (2006) 1791–1795.
[16] N. Maffei, L. Pelletier, J.P. Charland, A. McFarlan, J. Power Sources 140 (2005) 264–267.
[17] G.G.M. Fournier, I.W. Cumming, K. Hellgardt, J. Power Sources 162 (2006) 198–206.
[18] L. Zhang, W. Yang, J. Power Sources 179 (2008) 92–95.
[19] A. Wojcik, H. Middleton, I. Damopoulos, J. Vanherle, J. Power Sources 118 (2003) 342–348.
[20] M. Ni, D.Y.C. Leung, M.K.H. Leung, Int. J. Hydrogen Energy 33 (2008) 5765–5772.
[21] A. Skodra, M. Ouzounidou, M. Stoukides, Solid State Ionics 177 (2006) 2217–2220.
[22] A.S. Chellappa, C.M. Fisher, W.J. Thomson, Appl. Catal. A Gen. 227 (2002) 231–240.
[23] S.F. Yin, B.Q. Xu, X.P. Zhou, C.T. Au, Appl. Catal. A Gen. 277 (2004) 1–9.
[24] E.N. Gobina, J.S. Oklany, R. Houghes, Ind. Eng. Chem. Res. 34 (1995) 3777–3783.
[25] M.R. Rahimpour, A. Asgari, J. Hazard. Mater. 153 (2008) 557–565.
[26] M.R. Rahimpour, A. Asgari, Int. J. Hydrogen Energy 34 (2009) 5795–5802.
[27] M.R. Johnson, A.R. Coderre, Int. J. Greenhouse Gas Contr. 8 (2012) 121–131.
[28] Y.M. Lin, M.H. Rei, Catal. Today 67 (2001) 77–84.
[29] M.R. Rahimpour, S. Ghader, Chem. Eng. Technol. 26 (2003) 902–907.
[30] R. Dittmeyer, V. Hollein, K. Daub, J. Mol. Catal. A Chem. 173 (2001) 135–184.
[31] M.H. Khademi, A. Jahanmiri, M.R. Rahimpour, Int. J. Hydrogen Energy 34 (2009) 5091–5107.
[32] M.H. Khademi, A. Jahanmiri, M.R. Rahimpour, Int. J. Hydrogen Energy 34 (2009) 4930–4944.
[33] M.R. Rahimpour, M. Bayat, Int. J. Hydrogen Energy 36 (2009) 6616–6627.
[34] M.R. Rahimpour, S.M. Jokar, J. Hazard. Mater. 209–210 (2012) 204–217.
[35] M.R. Rahimpour, Z. Jamshidnejad, S.M. Jokar, G. Karimi, A. Ghorbani, A.H. Mohammadi, J. Nat. Gas Sci. Eng. 4 (2012) 17–28.
[36] J. Jia, Q. Li, M. Lou, L. Wei, A. Abudula, Energy 36 (2011) 1068–1075.
[37] Ammonia Plant Operating Data, Razi Petrochemical Complex, Iran, 2006.
[38] M. Temkin, V. Pyzhev, Acta Physicochim. URRS 12 (1940) 327–356.
[39] J.P. Collins, J.D. Way, N. Kraisuwansarn, J. Membr. Sci. 77 (1993) 265–282.
[40] R.H. Harrison, K.A. Kobe, Chem. Eng. Prog. 49 (1953) 349–353.
[41] J. Xu, G.F. Froment, AIChE J. 35 (1989) 88–96.
[42] Z. Arab Aboosadi, M.R. Rahimpour, A. Jahanmiri, Int. J. Hydrogen Energy 36 (2011) 2960–2968.
[43] R.C. Hurlburt, J.O. Konency, J. Chem. Phys. 34 (1961) 655–658.
[44] F.J. Ackerman, G.J. Koskinas, J. Chem. Eng. Data 17 (1972) 51–55.
[45] H. Yoshida, S. Konishi, Y. Naruse, J. Less-Common. Met. 89 (1983) 429–436.
[46] J. Chabot, J. Lecomte, C. Grumet, J. Sannier, Fusion Technol. 14 (1988) 614–618.
[47] S.A. Hajimolana, M.A. Hussain, M.W.A. Wan Daud, M. Soroush, A. Shamiri, Renew. Sustain. Energy Rev. 15 (2011) 1893–1917.
[48] M. Ni, M.K.H. Leung, D.Y.C. Leung, Energy Convers. Manag. 48 (2007) 1525–1535.
[49] M. Ni, D. Leung, M. Leung, J. Power Sources 183 (2008) 682–686.
[50] S. Kakaç, A. Pramuanjaroenkij, X.Y. Zhou, Int. J. Hydrogen Energy 32 (2007) 761–786.
[51] P. Chinda, S. Chanchaona, P. Brault, W. Wechsatol, J. Sustain. Energy Environ. 1 (2010) 185–196.
[52] P. Aguiar, C.S. Adjiman, N.P. Brandon, J. Power Sources 138 (2004) 120–136.
[53] Y. Patcharavorachot, W. Paengjuntuek, S. Assabumrungrat, Z. Arpornwichanop, Int. J. Hydrogen Energy 35 (2010) 4301–4310.
[54] S.H. Chan, K.A. Khor, Z.T. Xia, J. Power Sources 93 (2001) 130–140.
[55] J.R. Ferguson, J.M. Fiard, R. Herbin, J. Power Sources 58 (1996) 109–122.
[56] W.A. Rogers, R.S. Gemmen, C. Johnson, M. Prinkey, M. Shahnam, Fuel Cell Science and Engineering Technology, ASME, 2003, pp. 517–520.
[57] R.E. Williford, L.A. Chick, Surf. Sci. 547 (2003) 421–437.
[58] J.W. Kim, A.V. Virkar, K.Z. Fung, K. Mehta, S.C. Singhal, J. Electrochem. Soc. 146 (1999) 69–78.